Available online at www.sciencedirect.com
SCIENCE DIRECT®
Journal of Non-Crystalline Solids 348 (2004) 44–50
JOURNAL OF NON-CRYSTALLINE SOLIDS
www.elsevier.com/locate/jnoncrysol

Clustering of rare earth in glasses, aluminum effect: experiments and modeling

A. Monteil [a,*], S. Chaussedent [a], G. Alombert-Goget [a], N. Gaumer [a], J. Obriot [a], S.J.L. Ribeiro [b], Y. Messaddeq [b], A. Chiasera [c], M. Ferrari [d]

[a] *Laboratoire POMA – UMR CNRS 6136, Université d'Angers, 2 bd Lavoisier, 49045 Angers cedex 01, France*
[b] *Instituto de Química, UNESP-CP 355-Zip, 14801-970 Araraquara, SP, Brazil*
[c] *Dip. di Fisica e INFM, CSMFO group Università di Trento, via Sommarive 14, 38050 Povo-Trento, Italy*
[d] *CNR-IFN, Institute of Photonics and Nanotechnologies, CSMFO group, via Sommarive 14, 38050 Povo-Trento, Italy*

Abstract

Luminescent spectra of Eu^{3+}-doped sol–gel glasses have been analyzed during the densification process and compared according to the presence or not of aluminum as a codoping ion. A transition temperature from hydrated to dehydroxyled environments has been found different for doped and codoped samples. However, only slight modifications have been displayed from luminescence measurements beyond this transition. To support the experimental analysis, molecular dynamics simulations have been performed to model the doped and codoped glass structures. Despite no evidence of rare earth clustering reduction due to aluminum has been found, the modeled structures have shown that the luminescent ions are mainly located in aluminum-rich domains. The synthesis of both experimental and numerical analyses has lead us to interpret the aluminum effect as responsible for differences in structure of the luminescent sites rather than for an effective dispersion of the rare earth ions.

PACS: 61.43.Bn; 61.43.Fs; 78.55.Qr; 42.70.Ce; 02.70.Ns

1. Introduction

Rare earth (RE) doped silica glasses are of particular interest for optical applications. In such materials, high concentrations of dopant are often necessary to achieve good efficiency. Although enough high concentrations cannot be reached with conventional glasses cooled from a melt, the sol–gel technique offers an alternative allowing RE concentrations up to 10%. However, even at lower concentrations, the RE emission properties are subject to the so-called concentration quenching. This limiting factor is generally attributed to the conjunction of RE ions clustering through RE–O–RE bonds with energy transfers between these clustered ions by a cross-relaxation mechanism or phonon-assisted energy transfer [1].

Among the different solutions that have been proposed to avoid clustering and consequently concentration quenching, one of the most efficient is the sol–gel codoping with chosen cations [2,3]. It has been shown that Al^{3+} is particularly efficient [2]. However aluminum is known to retain water molecules and hydroxyl groups (OH^-) [1]. In producing optical materials by sol–gel technique, the removal of residual OH is a challenge. OH^- ions have a strong absorption band in the infrared region and their presence near RE ions causes fluorescence quenching by a fast non-radiative relaxation process.

However, the efficiency of the aluminum codoping to limit the concentration quenching results from

* Corresponding author: Tel.: +33 241735361; fax: +33 241735216.
E-mail address: monteil@univ-angers.fr (A. Monteil).

0022-3093/$ - see front matter © 2004 Elsevier B.V. All rights reserved.
doi:10.1016/j.jnoncrysol.2004.08.124

mechanisms that are still not clearly explained. This work is an attempt to better understand the aluminum effect on the material structure and on the spectroscopic properties. We report spectroscopic results on the first stages of the drying and densification processes in comparing Eu^{3+}-doped and Eu^{3+}/Al^{3+}-codoped sol–gel SiO_2 glasses. Numerical simulations using the molecular dynamics (MD) technique have been also performed for doped and codoped silica glass models in order to support the experimental analysis and to inspect the structural modifications due to the aluminum codoping.

2. Experimental

2.1. Samples preparation

Silica gels were prepared via hydrolysis and condensation of tetramethoxy-silane (TMOS), methanol (MeOH) and deionized water, in the presence of nitric acid. Europium and aluminum were introduced in the initial stage of the process, by dissolving hydrated europium nitrate $Eu(NO_3)_3 \cdot 5H_2O$ and hydrated aluminum nitrate $Al(NO_3)_3 \cdot 9H_2O$ in the mixture of HNO_3 and water. The molar ratio in the initial solution was 1:6:10:0.6 for TMOS:MeOH:H_2O:HNO_3. Several samples were prepared with the nominal compositions $x EuO_{1.5}$–$y AlO_{1.5}$–SiO_2, $x = 0.01$ (sample without aluminum) and $x = 0.01$, $y = 6x$ (sample with aluminum). The solution of all ingredients was stirred for some minutes and transferred into plastic beakers. The closed beakers were kept at 60 °C for five days and heated to 80 °C for one day. Gelation and aging of the samples took place within this period. The covers were then unscrewed to allow vaporization of the residual solvents, and the samples were dried for five weeks at room temperature. Next, the samples were transferred into an oven and sintered in air using a heating rate of 0.1 °C/min up to different final temperatures. The samples were kept for 10 h at these temperatures and finally cooled to room temperature.

2.2. Experimental set-up

The 355 nm line of a Nd-YAG laser was used for excitation in lifetime and photoluminescence measurements. Fluorescence was focused on the entrance slit of a Jobin-Yvon THR 1500 spectrometer and detected by a cooled R943-02 Hamamatsu photomultiplier tube (PMT). The PMT was connected to photon-counting electronics. Lifetime measurements were performed with a multichannel analyzer Stanford SR430 via a fast amplifier discriminator (Stanford SR445) with a minimum channel width of 5 ns. All measurements were done at room temperature.

2.3. Numerical simulations

Using the MD technique we have simulated two numerical glass samples: $18Er_2O_3 \cdot 1698SiO_2$ and $18Er_2O_3 \cdot 108Al_2O_3 \cdot 1446SiO_2$. A Verlet algorithm has been employed to integrate the classical Newton equations of motion dealing with boxes of about 5000 atoms. The interatomic potential used in this simulation is the same form as that developed by Feuston and Garofalini [4]. This potential is composed of two parts: the two-body term describes the interaction between atomic pairs while the three-body term is employed to take into account the covalence of the Si–O and Al–O bonds. The two-body part is given by

$$V_{ij}(r_{ij}) = A_{ij}\exp(-r_{ij}/\rho_{ij}) + \mathrm{SCP},$$

where r_{ij} is the distance between particles i and j, and SCP stands for screened Coulombian potential. According to atomic triplets, the three-body potential is chosen between these two expressions:

$$V_1(\theta_{ijk}, r_{ij}, r_{ik}) = \lambda_{ijk}\exp\left(\frac{\gamma_{ij}}{r_{ij} - r_{ij}^0}\right) \times \exp\left(\frac{\gamma_{ik}}{r_{ik} - r_{ik}^0}\right)\left(\cos\theta_{jik} - \cos\theta_{jik}^0\right)^2,$$

$$V_2(\theta_{ijk}, r_{ij}, r_{ik}) = \lambda_{ijk}\exp\left(\frac{\gamma_{ij}}{r_{ij} - r_{ij}^0}\right)\exp\left(\frac{\gamma_{ik}}{r_{ik} - r_{ik}^0}\right) \times \left[\left(\cos\theta_{jik} - \cos\theta_{jik}^0\right)\sin\theta_{jik}\cos\theta_{jik}\right]^2,$$

where r_{ij} (respectively r_{ik}) is the distance between particles i and j (respectively i and k), θ_{jik} is the angle between particles j, i, k. Other constants are parameters that are reported in Table 1.

The following common process was used to produce the simulated samples: an initial configuration is firstly melted at 12 000 K for 80 ps to ensure a perfect mixing of the system. Melts are then cooled to room temperature to give glassy structures in nine successive temperature steps. First applications of the MD technique used to model rare-earth doped silicate glasses were presented in 1993 by Capobianco and his group [5]. Details on the procedure used here can be found in Ref. [6]. The structure of the simulated glasses has been studied by means of the radial distribution functions (RDF) and various ad hoc computational procedures including cluster statistics.

The reason why erbium instead of europium has been chosen as doping ion in the simulated glasses is that adjustments of the potential parameters have to be supported by experimental data such as EXAFS measurements. Since erbium is often used for its applied properties, interatomic distances and coordination numbers are available in the literature [7]. However, erbium

Table 1
Parameters for two-body and three-body potentials

	Er–O	Er–Si	Er–Al	Er–Er	Al–O	Al–Si	Al–Al	Si–O	Si–Si	O–O
A_{ij} (eV)	105	624	624	1025	1734	961	1100	1849	1172	453
ρ_{ij} (Å)	0.21	0.29	0.29	0.29	0.29	0.29	0.29	0.29	0.29	0.29

j–i–k	Potential	λ_{jik} (eV)	θ^0_{jik} (°)	$\gamma_{ij} = \gamma_{ik}$ (Å)	$r^0_{ij} = r^0_{ik}$ (Å)
Al–O–Al	V_1	6.2	109.5	2.0	2.6
O–Al–O	V_2	150	109.5	2.8	3.0
Si–O–Si	V_1	6.2	109.5	2.6	3.0
O–Si–O	V_1	150	109.5	2.6	3.0

is not ideal as a structural probe in spectroscopic experiments whereas, on the contrary, europium presents a particular sensitivity to the crystal field and offers relatively simple spectroscopic features. Assuming that the structural behavior of erbium and europium as doping ions in such glasses should be similar, we consider that the results obtained from the simulated erbium-doped glasses can be interpreted in conjunction with those of the luminescence experiments performed on the europium-doped glasses.

3. Results

The different densification stages of a gel to a glass have been investigated using europium emission as a photoluminescent probe. Eu^{3+} shows an emission spectrum composed of several multiplet transitions $^5D_0 \rightarrow {}^7F_{J=0,1,\ldots,6}$. The first transition, $^5D_0 \rightarrow {}^7F_0$, is spin-forbidden and only allowed by J-mixing effects. Its position and shape are very sensitive to the electrostatic field generated by the local structure. The second transition, $^5D_0 \rightarrow {}^7F_1$, is mainly magnetic dipolar and intensity-insensitive to the local field, but it shows a splitting feature directly proportional to the crystal field strength. The intensity of the third one, $^5D_0 \rightarrow {}^7F_2$, depends drastically on the crystal field strength. Figs. 1 and 2 show the evolution of the emission spectrum during the transition from the gel to the glass for the doped (Fig. 1) and the aluminum codoped (Fig. 2) samples. Dramatic changes in the spectra (positions, splitting and intensities) can be observed and indicate that an important modification in the local environment occurs at a given treatment temperature. One can note that this threshold temperature depends on the presence of aluminum. Particularly, for the doped sample, a line broadening occurs around 150 °C, whereas the same broadening is delayed up to a temperature of 300–350 °C for the codoped sample. The same evolution can be observed for the splitting of the $^5D_0 \rightarrow {}^7F_1$ transition. Beyond these threshold temperatures, no dramatic changes are displayed.

In order to quantify these effects we have calculated the second order crystal field coefficients, B_{20} and B_{22}

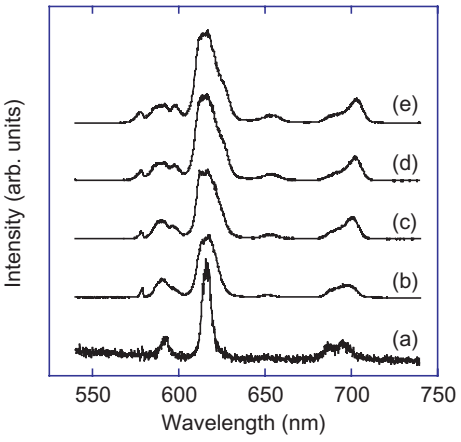

Fig. 1. Emission spectra (room temperature) of 1 at.% Eu^{+3}-doped sol–gel silica at various heat-treatment temperatures, excited at 355 nm. Intensities were normalized to the $^5D_0 \rightarrow {}^7F_1$ emission. Temperatures: (a) 80 °C, (b) 150 °C, (c) 250 °C, (d) 350 °C, (e) 900 °C.

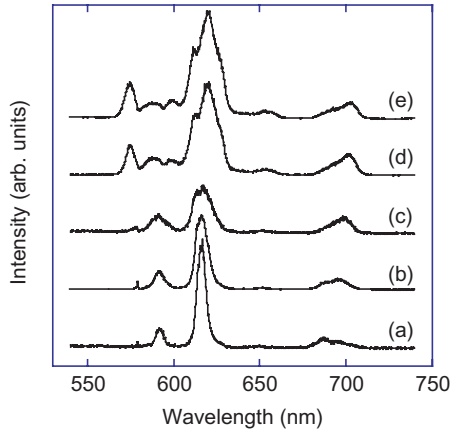

Fig. 2. Emission spectra (room temperature) of 1 at.% Eu^{+3}–6 at.% Al^{3+}-codoped sol–gel silica at various heat-treatment temperatures, excited at 355 nm. Intensities were normalized to the $^5D_0 \rightarrow {}^7F_1$ emission. Temperatures: (a) 80 °C, (b) 150 °C, (c) 250 °C, (d) 350 °C, (e) 900 °C.

from the maximum line positions of the $^5D_0 \rightarrow {}^7F_1$ components: $B_{20} = -5/3(E_+ + E_- - 2E_0)$ and $B_{22} = 5/\sqrt{6}(E_- - E_+)$ where $E_\pm$ and E_0 denote the component energies. Then, the second order crystal field strength

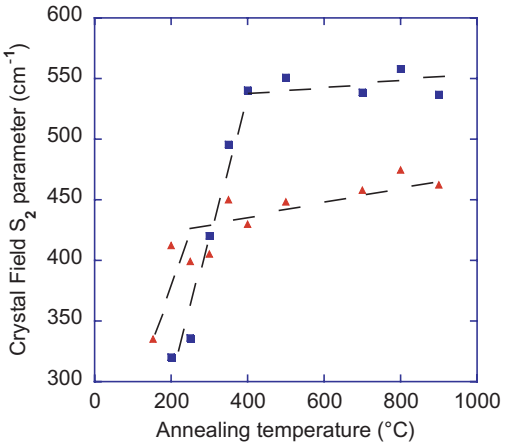

Fig. 3. Crystal field strength S_2 calculated from the peak positions of the $^5D_0 \rightarrow {}^7F_1$ transitions in the 1 at.% Eu^{+3}-doped (▲) and in the 1 at.% Eu^{+3}–6 at.% Al^{3+}-codoped sol–gel silica (■) at various heat-treatment temperatures. Dashed lines are drawn as a guide for eye.

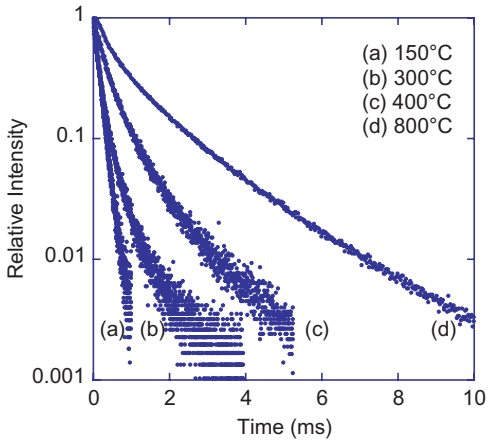

Fig. 5. Normalized decay curves of the Eu^{3+}–Al^{3+}-codoped samples at different heat treatment. The excitation and emission wavelengths are 355 and 620 nm, respectively.

parameter can be deduced as follows: $S_2 = \sqrt{\frac{1}{5}(B_{20}^2 + 2B_{22}^2)}$. Fig. 3 shows the variations of S_2 with temperature treatment both for the doped and codoped samples.

Changes during the densification processes have been already studied in detail for silica sol–gel in previous works [1,8,9]. Particularly some of the modifications have been related to the removal of water and OH groups owing to the thermal treatment [1,10]. Differences between doped and codoped silica sol–gel have been also reported [1,3]. An important effect of aqueous environments is the quenching of luminescence, OH vibration modes playing the role of traps. Analysis of luminescence decays can help for the interpretation of energy transfers and quenching processes. Figs. 4 and 5 show the decay curves of the $^5D_0$ level recorded from the $^5D_0 \rightarrow {}^7F_2$ emission for different treatment temperatures. Whereas for the Eu^{3+}-doped sample the evolution from a fast almost exponential decay (0.15 ms) to a slow almost exponential decay (1.5 ms) is progressive, for the Eu^{3+}–Al^{3+}-codoped sample decays are no longer exponential and a slower tail appears clearly for temperatures higher than 400 °C (2.2 ms at 800 °C).

In order to understand the differences generated by the presence of aluminum, the microscopic structure has been analyzed from statistics on the simulated samples. Fig. 6 shows the first peak of the Er–O RDF together with the associated cumulative distribution function (CDF) for both the doped and aluminum codoped numerical samples. The maximum position of the RDF first peak gives 2.38 and 2.40 Å as Er–O bonding distance for the doped and the codoped samples, respectively. At 3.00 Å, the plateau of the CDF curve gives 5.55 and 5.70 as oxygen coordination number for Er^{3+} in doped and codoped samples, respectively. Be-

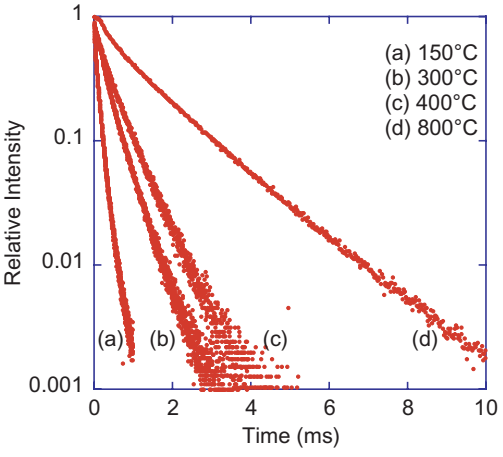

Fig. 4. Normalized decay curves of the Eu^{3+}-doped samples at different heat treatment. The excitation and emission wavelengths are 355 and 620 nm, respectively.

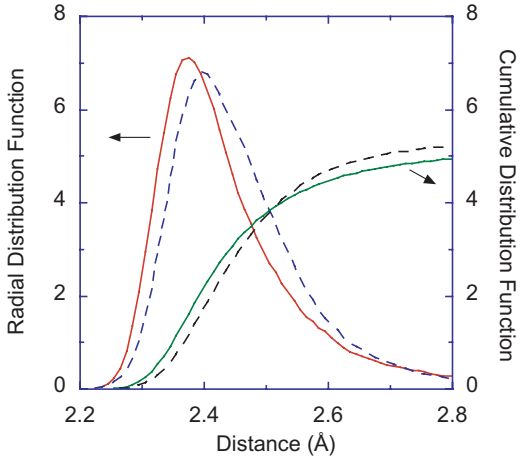

Fig. 6. Er–O radial distribution functions (RDF) and cumulative distribution functions (CDF) for the Er-doped silica network and the Er–Al-codoped silica network.

sides the lengthening of the RE–O distance, aluminum seems to be responsible for a broadening of the RDF first peak. In order to explain this effect, the Er–O RDF has been calculated in separating contributions due to the different kinds of oxygen accordingly to its bonding with the second coordination shell. An oxygen atom of the first coordination shell of erbium can be linked with an other erbium ion, with a silicon or an aluminum ion, or be a bonding oxygen when linked with two cations. Fig. 7 displays these different contributions and shows that Er–O–Si linkages are very few in number and are responsible for the shortest Er–O distance (2.38 Å), whereas the longest distance (2.42 Å) is achieved with bonding oxygen.

In Fig. 8, a snapshot of the aluminum codoped simulated structure is drawn and shows clearly that erbium ions are situated in aluminum-rich domains. However, the aluminum codoping does not seem to prevent erbium clustering since such clusters are still clearly identifiable.

From the particles positions in the simulated glass structures, we have calculated the second order crystal field parameters using a point charge model. The distribution of the S_2 values for every erbium sites is plotted in Fig. 9. The codoped structure is clearly distinguishable from the doped one by a double distribution of the S_2 values. This double distribution could not be related to the presence or absence of Al in the RE neighborhood, neither to a clustering effect. In discriminating erbium sites presenting the highest energy parameters from those presenting the lowest ones, we have plotted in Fig. 10 the Er–O–Si angular distribution function that reveals an important structuring effect. Structurally speaking, the modifications that aluminum induces in the RE neighborhood appear to be a reorganization of atoms owing to more defined distances and angles. The so-defined new sites correspond to high energy sites. This should have consequences on the spectroscopy.

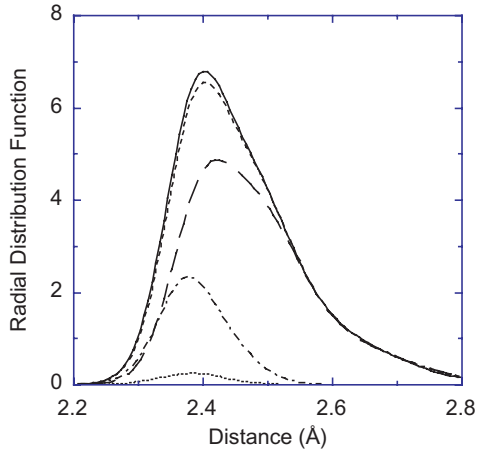

Fig. 7. Er–O RDFs for Er–Al-codoped sample. We distinguish different linkages Er–O–M, where M is a cation (Er, Al or Si): (continuous line) any kind of linkage, (small dash) M = Al or Er, (dot) M = Si, the sum of these two last curves give the continuous line, (long dash) bonding oxygen (M = 2 cations), (dash and dots) non-bonding oxygen (M = 1 cation), the sum of these two last curves give the continuous line.

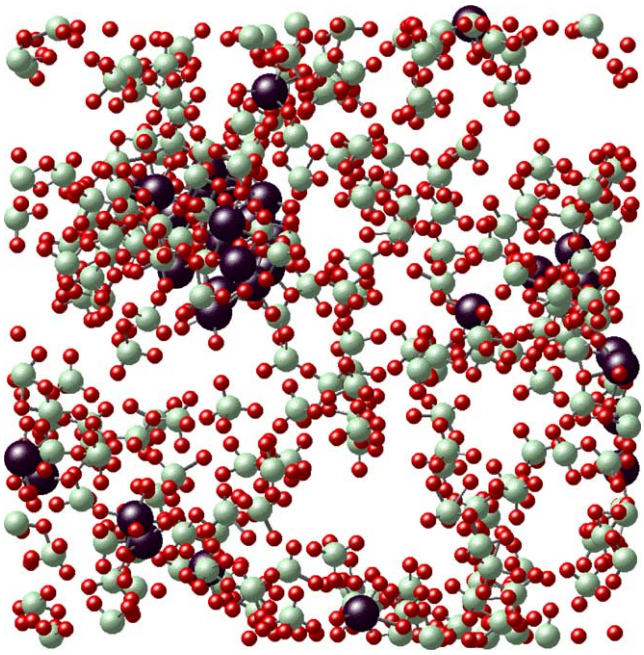

Fig. 8. Snapshot of a Er–Al-codoped silica simulated structure. Large black atoms are Er, light gray atoms are Al and small black ones are O. Only oxygen bonded to erbium or aluminum are represented. Silicon atoms are not represented for the sake of clarity.

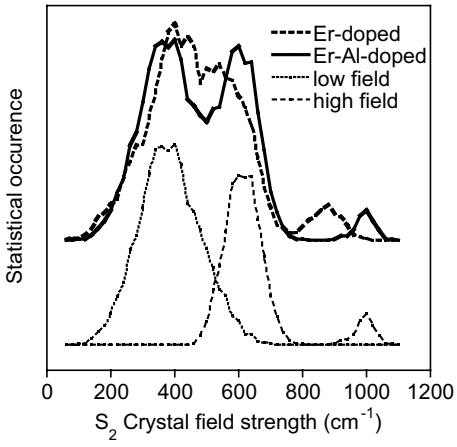

Fig. 9. S_2 crystal-field strength for Er-doped (dashed line) and Er–Al-codoped silica (continuous line). For the codoped sample a double distribution of sites at low energy (dot) and high energy (small dash) is distinguished for further calculations.

4. Discussion

From spectroscopic results, the first evidence is that aluminum has an important influence on the sensitive rare earth. Shape of lines and relative intensities

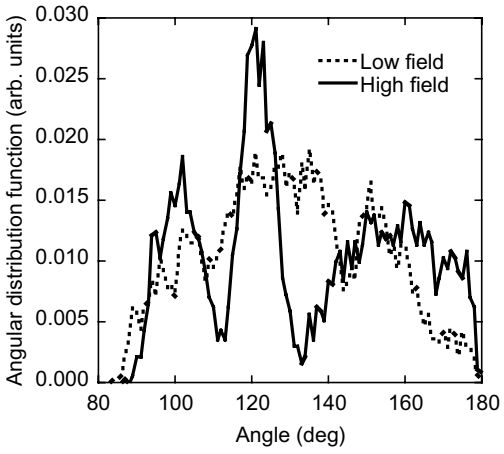

Fig. 10. Er–O–Si angular distribution function for Er–Al-codoped silica. Continuous line is for the higher energy sites and dashed line for the lower ones.

are different for the doped and the codoped samples. Aluminum changes the microscopic structure near the RE ion since its luminescence spectrum is completely modified. Costa et al. have already discussed on the modifying cations effect [2]. They interpreted this effect as a change in the covalence of Eu–O bonds. Such spectroscopic modifications are important and saturated: they do not change at low concentrations of Al [1]. This could be due to a good affinity between Al and RE bringing them closer together, or to an influence of Al at larger distances. Results of the simulation support the idea of a good affinity since RE ions prefer Al-rich domains as it can be seen on the snapshot of Fig. 8 while the average Er–Al coordination was found to be 2. This is consistent with the model developed by Laegsgaard [11].

The second point is that the drastic modifications in the luminescent spectrum occur at a higher temperature of treatment for the codoped sample. In RE-doped alumina, Ishizaka et al. [12] have noted that 'at 25–400 °C, heat-treatment results in the elimination of OH groups strongly bonded on alumina and this simultaneously accompanies changes of the alumina matrix and the conditions around rare earth ions'. As soon as the main part of OH groups is eliminated the spectroscopic characteristics do not change a lot with the temperature, even at temperature where the gel is not completely densified and remains porous. In fact changes are then more quantitative than qualitative, since evolutions at higher temperatures are less important. From the RE point of view, the observed transition can be interpreted as a change from an aqueous environment to a cationic dominated one at a temperature depending on the codoping cation.

Since spectra features are sensitive to the crystal field, which is due to the surrounding environment acting as a distribution of charges, we can conclude that the local environment of the RE ions, their relative positions with aluminum and silicon, are well established above the transition temperature.

In addition to the emission spectra, the decay curves can also be related to the structural environment through the Judd–Ofelt model. Lifetimes of the emitting levels are equally sensitive to non-radiative and energy transfer processes. The measured decay curves show a constant evolution during the different stages of the heat treatment. For the codoped sample decays are strongly non-exponential. A strong inhomogeneous character of the transitions can explain this shape: each site contributes with a slightly different decay rate. The quasi-exponential decays observed for the doped sample is consistent with an absence of fluorescence line narrowing (FLN) effect: fast energy transfer mechanisms among the clustered RE ions lead to an averaged decay time [2]. It can also be interpreted as a more homogeneous character of the transitions. The presence of aluminum in the vicinity of the RE ions would favor a wider range of experienced environments, i.e. of very different possible crystal fields.

Commonly, the concentration quenching is attributed to clusters formation whereas the aluminum effect is interpreted as favoring the cluster dispersion [3]. A previous investigation on the microscopic structure of RE-doped silicate networks has given evidence of the clustering trend [13]. But this study has not revealed a clear dispersion effect in the aluminum codoped matrix. First of all, this could result from inadequacies of our model and simulations. However, aluminum effect on the RE ions is manifest in the simulated structures. The first point is that aluminum is never located far from the RE ions. Consequently, the proportion of bonding oxygen (for instance Al–O–Si linkage) in the RE first coordination shell is increased and the mean distance between RE and oxygen becomes longer in the codoped sample than in the doped one. From EXAFS measurements, Rocca et al. have found an increase of the Er–O distance from 2.32 Å to 2.37 Å, to be compared with the increase from 2.38 Å to 2.40 Å determined from our simulated structures (Fig. 6) [7]. Despite a disagreement on these absolute values, which could be due to inadequacies of the simulated model and to accuracy in EXAFS measurements, an increase of the bonding length is meaningful. Thus, the aluminum codoping seems to influence every RE ion in the glass. The relationship between structure and spectroscopy has been investigated through crystal field parameters. From the experimental spectra, the deduced crystal field strength has given higher values for the codoped sample, that is directly linked to the larger splitting of the $^5D_0 \rightarrow {}^7F_1$ transition. On the other hand, the FLN experiments performed by Lochhead et al. have pointed out different kinds of spectroscopic site which can experience whether a higher or a lower crystal field energy [1,2]. In agreement with this experimental result, the

crystal field strength distribution obtained from the simulated codoped structure is clearly composed of two contributions: a high and a low energy contributions which can be associated to two different kinds of spectroscopic site (Fig. 9). In comparing the local structure of these two kinds of site, aluminum location do not seem to play a discriminating role. However, the examined structures reveal a different structuring effect according to the energy of the sites: the angular distribution function of Fig. 10 shows that the highest energy sites present more defined bonding angles, as it would be in a crystalline phase.

In the light of these results, it appears that aluminum codoping is responsible for an anti-quenching effect through a local modification of the RE environments rather than through a physical cluster dispersion. In structuring the RE local environments, aluminum increases the differences in the diversity of sites which also leads to a wider range of decay rates and consequently reduces the resonant energy transfer mechanisms.

5. Conclusion

The effect of aluminum codoping in rare-earth-doped silica glasses was investigated using both spectroscopy of samples prepared by the sol–gel technique and analysis of numerical structures simulated by the molecular dynamics technique. Photoluminescence spectra and decay curves have pointed out a transition in the evolution of the glass structure during the densification process. This transition occurs at a treatment temperature which is higher for the codoped sample. The first effect of aluminum codoping is thus to delay the dehydroxylation mechanism. Above this transition temperature, modifications become slighter and one can consider that the structure is well established.

From numerical simulations, the aluminum effect on the densified structure has been interpreted in term of affinity between RE and Al ions. The medium range structure shows that RE ions are preferentially located in aluminum-rich domains, while the local structure around RE ions is affected by aluminum through a structuring effect.

Our interpretation of the aluminum anti-quenching effect is therefore a modification of the RE local structure toward a pre-crystalline phase rather than a cluster dispersion ability as it is commonly supposed.

Acknowledgments

Authors acknowledge the financial support of Conseil Général de Maine-et-Loire and Angers-Agglomération, MIUR-FIRB 'Sistemi miniaturizzati per elettronica e fotonica (RBNE0112N3X)', MIUR-Cofin 2002 'materiali nanostrutturati per l'ottica integrata', and FAPVU project Fondo Unico per il sostegno alla ricerca, Provincia Autonoma di Trento. This work was performed within a CNRS (France) – CNR (Italy) cooperation and a CNRS (France) – CNPq (Brazil) cooperation. A DLPOLY package from the Council for the Central Laboratory of the Research Council, Daresbury Laboratory has been used.

References

[1] M.J. Lochhead, K.L. Bray, Chem. Mater. 7 (1995) 572.
[2] V.C. Costa, M.J. Lochhead, K.L. Bray, Chem. Mater. 8 (1996) 783.
[3] K. Arai, H. Namikawa, K. Kumata, T. Honda, Y. Ishii, T. Handa, J. Appl. Phys. 59 (1986) 3430.
[4] B.P. Feuston, S.H. Garofalini, J. Chem. Phys. 89 (1988) 5818.
[5] See e.g. G. Cormier, J.A. Capobianco, A. Monteil, J. Non-Cryst. Solids 152 (1993) 225;
T. Peres, D.A. Litton, J.A. Capobianco, S.H. Garofalini, J. Non-Cryst. Solids 221 (1997) 34.
[6] S. Chaussedent, C. Bernard, A. Monteil, N. Balu, J. Obriot, S. Ronchin, C. Tosello, M. Ferrari, Proc. SPIE 3942 (2000) 243.
[7] F. Rocca, M. Ferrari, A. Kuzmin, N. Daldosso, C. Duverger, F. Monti, J. Non-Cryst. Solids 293–295 (2001) 112.
[8] B. Andrianasolo, M. Ferrari, A. Monteil, E. Duval, A. Serughetti, R. Campostrini, G. Carturan, M. Montagna, F. Rossi, J. Phys. IV-C7 7 (1) (1991) 501.
[9] M.J. Lochhead, K.L. Bray, J. Non-Cryst. Solids 170 (1994) 143.
[10] B.T. Stone, V.C. Costa, K.L. Bray, Chem. Mater. 9 (1997) 2592.
[11] J. Laegsgaard, Phys. Rev. B 65 (2002) 174114.
[12] T. Ishizaka, R. Nozaki, Y. Kurokawa, J. Phys. Chem. Solids 63 (2002) 613.
[13] C. Bernard, S. Chaussedent, A. Monteil, Philos. Mag. B 82 (2002) 681.